ARTICLE IN PRESS

Icarus xxx (2016) xxx–xxx

Contents lists available at ScienceDirect

Icarus

journal homepage: www.journals.elsevier.com/icarus

Role of fluids in the tectonic evolution of Titan

Zac Yung-Chun Liu [a,b,*], Jani Radebaugh [a], Ron A. Harris [a], Eric H. Christiansen [a], Summer Rupper [a,c]

[a] Department of Geological Sciences, Brigham Young University, Provo, UT 84602, USA
[b] Now at School of Earth and Space Exploration, Arizona State University, Tempe, AZ 85287, USA
[c] Now at Department of Geography, University of Utah, Salt Lake City, UT 84112, USA

ARTICLE INFO

Article history:
Received 23 July 2015
Revised 5 January 2016
Accepted 6 February 2016
Available online xxxx

Keyword:
Titan, surface
Tectonics
Geological processes
Titan, hydrology

ABSTRACT

Detailed analyses of slopes and arcuate planform morphologies of Titan's equatorial mountain ridge belts are consistent with formation by contractional tectonism. However, contractional structures in ice require large stresses (4–10 MPa), the sources of which are not likely to exist on Titan. Cassini spacecraft imagery reveals a methane-based hydrological cycle on Titan that likely includes movement of fluids through the subsurface. These crustal liquids may enable contractional tectonic features to form as groundwater has for thrust belts on Earth. In this study, we show that liquid hydrocarbons in Titan's near subsurface can lead to fluid overpressures that facilitate contractional deformation at smaller stresses (<1 MPa) by significantly reducing the shear strength of materials. Titan's crustal conditions with enhanced pore fluid pressures favor the formation of thrust faults and related folds in a contractional stress field. Thus, surface and near-surface hydrocarbon fluids made stable by a thick atmosphere may play a key role in the tectonic evolution of Titan.

1. Introduction

Titan, the largest moon of Saturn, has a thick atmosphere, surface fluids (Stofan et al., 2007; Lorenz et al., 2008), subsurface liquids (Hayes et al., 2008), and a methane-based hydrologic cycle that likely includes a ground 'methane' system similar to Earth's groundwater system (Lunine and Lorenz, 2009). The stability of fluids on and near the surface makes Titan unique among the satellites that have icy lithospheres. Since the Cassini spacecraft (2004–present) began imaging Titan's surface, many studies have examined the Earth-like geological processes involving surface fluids (e.g., Hayes et al., 2008; Lunine and Lorenz, 2009; Burr et al., 2013). It is also possible to examine the role of subsurface fluids in the tectonic evolution of the lithosphere, despite the fundamental rheological differences between materials of Earth and Titan (i.e., liquid hydrocarbon in water ice crust).

The general understanding of icy satellite tectonics is that most bodies exhibit evidence for extensional tectonism (e.g., fractures, grabens, normal faults), whereas evidence for contractional tectonism (e.g., folds, thrust faults) is rare (Collins et al., 2009). The stress required to form contractional structures in ice on Ganymede and Europa is estimated at 10–25 MPa (Dombard and McKinnon, 2006; Pappalardo and Davis, 2007), 3–8 times that required to form extensional features in ice. Generating such large stresses on icy satellites is difficult. The dominant source of stress for brittle-frictional faulting, which is diurnal eccentricity, can only generate stresses of 0.1 MPa on Europa and <0.1 MPa on Ganymede and Titan (Collins et al., 2009). It is possible that other mechanisms may produce larger stresses, such as despinning, non-synchronous rotation, polar wander (e.g., Dombard and McKinnon, 2006), or volume change (Mitri et al., 2010a,b), but in the absence of these mechanisms, sources of contractional stress sufficient for thrust faulting probably do not exist on most icy satellites, including Titan.

Nevertheless, there is strong evidence that contractional features do exist on Titan. The Cassini RADAR instrument, operating in Synthetic Aperture Radar (SAR) mode, has obtained images at ~350 m resolution of many landforms on Titan (Elachi et al., 2005; Lunine et al., 2008), including E–W oriented, long, narrow mountain ridges (Fig. 1) (Radebaugh et al., 2007; Cook-Hallett et al., 2015; Liu et al., this issue). Their long, curvilinear morphology (Paganelli et al., 2010; Radebaugh et al., 2011; Solomonidou et al., 2013; Liu et al., this issue), their low slopes and relief (Radebaugh et al., 2007; Liu et al., 2012; Mitri et al., 2010a), comparisons of these morphologies with Earth's tectonic features (Solomonidou et al., 2013), and structural and stress field analysis (Paganelli et al., 2010; Cook-Hallett et al., 2015; Liu et al., this issue) are all consistent with formation by contraction. However,

* Corresponding author at: School of Earth and Space Exploration, Arizona State University, ISTB4-745, Tempe, AZ 85287, USA.
E-mail address: zacycliu@asu.edu (Z.Y.-C. Liu).

http://dx.doi.org/10.1016/j.icarus.2016.02.016
0019-1035/

Please cite this article in press as: Liu, Z.-Y.C., et al. Role of fluids in the tectonic evolution of Titan. Icarus (2016), http://dx.doi.org/10.1016/j.icarus.2016.02.016

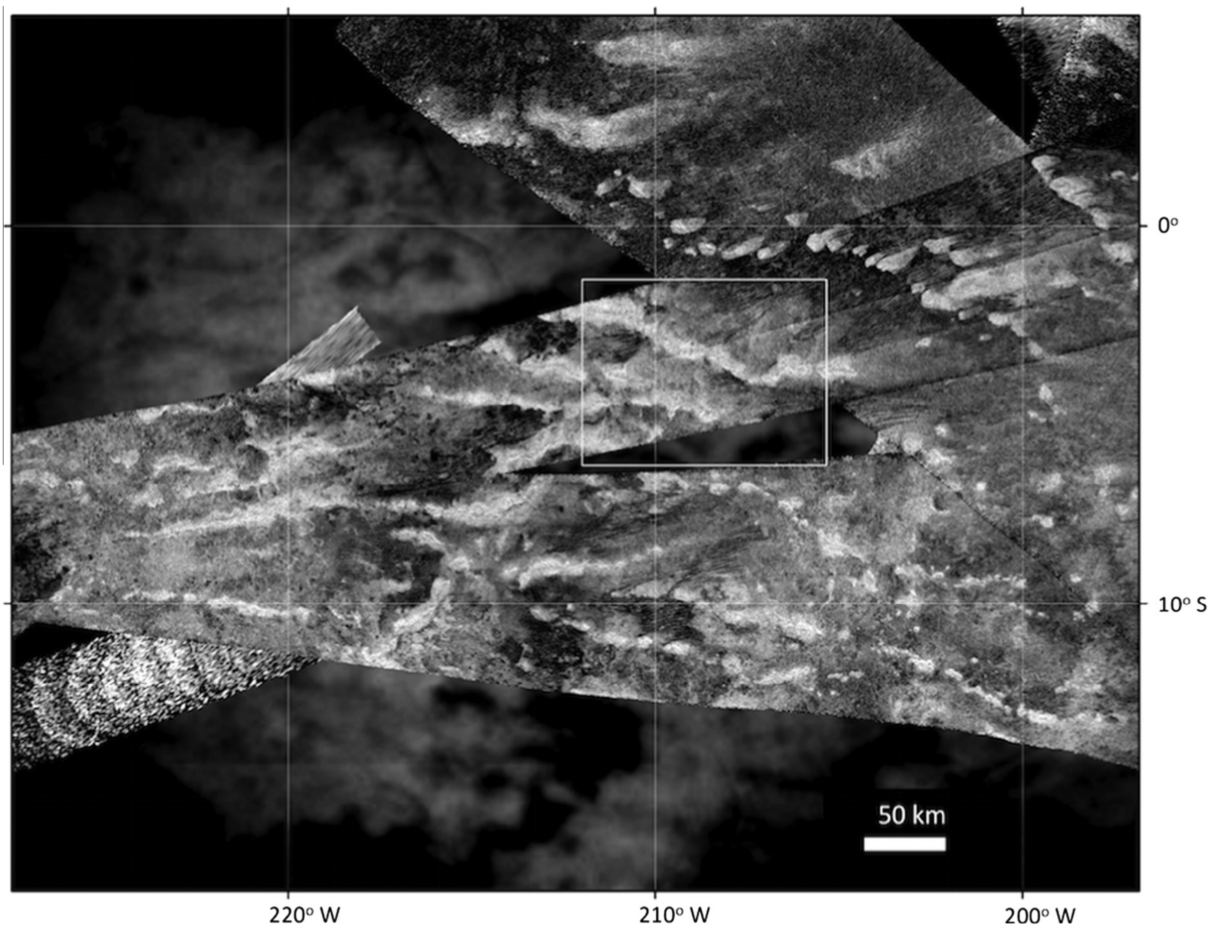

Fig. 1. Mountain ridge belts on Titan. Bright linear ridges at 200–230°W, 5°N–15°S are apparent on this image, which is a Cassini SAR (Synthetic Aperture Radar) mosaic (T8, T61 and T41 flyby swaths) processed using Imaging Science Subsystem (ISS). SAR image brightness represents the normalized microwave energy backscattered from the surface, which is a function of surface slope, dielectric properties, roughness, and the amount of volume scattering. Ridge belts are elevated, SAR-bright features with curvilinear margins morphologically similar to terrestrial fold belts. White rectangle shows the location of the image in Figs. 2 and 6.

the source of stresses large enough to produce the contractional structures is not obvious.

1.1. The origin of Titan's tectonism

Both Cook-Hallett et al. (2015) and Liu et al. (this issue) documented Titan's global tectonic pattern by mapping outlines of mountains and traces of ridges, respectively. Both studies revealed a pattern of E–W oriented mountains and ridges within 30° of the equator. Cook-Hallett et al. (2015) found mountains oriented N–S between 60° latitude and the poles, while Liu et al. (this issue) contend the ridges trend E–W globally. Both studies concluded that Titan's global tectonic pattern could be caused by contractional tectonism. Liu et al. (this issue) suggested global contraction with initial lithospheric thinning in the equatorial regions (Beuthe, 2010) could explain the global tectonic pattern. Cook-Hallett et al. (2015) suggested that either global contraction coupled with spin-up or global expansion coupled with despinning could explain the pattern if coupled with a thin lithosphere in Titan's polar regions. However, the magnitude of stress calculated from their model is <0.1 MPa (Cook-Hallett et al., 2015), which is much lower than would be expected for thrust fault formation. A model for contraction on Titan by Mitri et al. (2010a,b) revealed that volume change resulting from internal cooling may possibly provide enough stress to form contractional folds on Titan, but their model does not account for the global tectonic pattern. Therefore, current geophysical models cannot explain both the global tectonic pattern and the source of large stresses to produce the contractional structures.

1.2. Goal of this study

This study explores the role of fluids and their effect on Titan's tectonic evolution, specifically on contractional tectonism. We report that fluid pressures associated with liquid hydrocarbons in Titan's subsurface significantly reduce the shear strength of the icy crust and enable contractional structures to form without the requirement of large stresses. Although the thermal model constructed by Mitri et al. (2010a,b) suggested that the volume change mechanism may possibly provide enough stress to form contractional structures on Titan, the fluid overpressures model extended in this study provides a way to significantly reduce the strength of Titan's crust and allow contractional deformation at much lower stresses.

In this paper, we first discuss new evidence supporting the model of contractional tectonism having built the equatorial ridge belts on Titan (Section 2). We then estimate the strength of Titan's icy lithosphere and the differential stress necessary for failure in the brittle and ductile regimes (Section 3). Finally, we discuss the role of fluid pore pressure on Earth and how it reduces the stress needed for contraction and address its application to Titan's unique crustal environment (Section 4). Notably, since the effect of fluid pore pressure in Titan's tectonic evolution has never been explored in previous studies, the initial first-order modeling we present here is to demonstrate the importance of fluid overpressure in facilitating contractional tectonism on Titan. More sophisticated numerical analysis is left for future study.

2. New evidence supporting contractional tectonism on Titan

2.1. Surface slope of ridges

Dynamic topography associated with active tectonics can be used to determine the first-order structural nature of some deformation features. For example, the average slope of fold and thrust belts on terrestrial planets is commonly <15° (e.g., Yakima fold-and-thrust belts in Washington, USA (Reidel, 1984) and lobate scarps on the Moon (Banks et al., 2012)). The slopes of mountain fronts formed by normal faults are commonly steeper >45° (e.g., Wasatch front in Utah, USA) where unmodified by erosion and deposition. Topographic profiles across ridge belts on Titan, perpendicular to the ridge strike (Fig. 2), were constructed using the SARTopo technique (Stiles et al., 2009), which obtains absolute topography with respect to the 2575 km radius sphere from overlapping Synthetic Aperture Radar (SAR) images. It enables two or more surface-height profiles to be obtained from the long dimension of each SAR image. The SARTopo profiles are narrow bands, not everywhere normal to ridge belt strikes. Thus, the average slopes (α') obtained from SARTopo profiles must be converted to true slope (α) through the simple relationship $\tan\alpha' = \tan\alpha \sin\delta$, where δ is the angle between the ridge strike and the SARTopo trace. The overall surface slope of the mountain ridges was determined from the ridge height (H) and width (W) (Fig. 2c) through $\alpha' \sim \tan^{-1}$ (H/W; Fig. 2a and b). The ridge crest was identified in SAR imagery as a bright/dark pair formed by the peak and its shadow. The mountain width (W) is determined by where the SAR-bright, fractured and rough mountain materials terminate at the valley floor. The elevation difference between the ridge crest and valley floor was used to obtain the ridge height (H) (Fig. 2c). Systematic errors and uncertainty in heights were determined from SAR instrument noise and viewing geometry, and are summarized in Stiles et al. (2009). SARTopo data have an average vertical uncertainty of 75 m and a horizontal uncertainty of 10 km (Stiles et al., 2009). By incorporating the systematic errors in the calculation of the height (H) (Fig. 2b), we calculated the uncertainty of the ridge height (H_L and H_U: lower and upper bound of ridge height) (Fig. 2c). Thus, an estimate of the surface slope (α) has a corresponding uncertainty range. Details on the measurement results can be found in Table 1.

The average surface slope of Titan's equatorial ridge belts obtained from SARTopo profiles is <2–8°, including the uncertainty in the measurements (Table 1). These low slopes suggest the ridges on Titan are most like fold-and-thrust belts rather than extensional normal faults. However, erosion and deposition may also have degraded the slopes on Titan, possibly biasing the results toward lower angle slopes. Black et al. (2012) and Tewelde et al. (2013) undertook quantitative analyses of the shapes of drainage networks and the sinuosity of polar lake shorelines on Titan, the results of which show spatially averaged fluvial erosion of 0.4–9% of the initial topographic relief globally and erosion of 4–31% of initial relief for polar regions. These results indicate that while fluvial erosion is a significant agent in landscape modification on Titan, it progresses far more slowly on Titan than on Earth, which may result in the long-term preservation of features such as rugged crater rims and mountain ridges (Black et al., 2012; Tewelde et al., 2013; Neish et al., this issue). Furthermore, mountain ridge morphologies on Titan likely evolved under coeval fluvial and tectonic processes, similar to mountains on Earth (e.g., Yakima fold-and-thrust belt, Washington, USA), where ridge slopes coupled with plan-view morphologies are used to ascertain stress orientations despite heavy fluvial modification (see Section 2.2). Currently it is not possible, with our image resolution, to see faults or offsets; nevertheless, the low-angle slopes and morphologies outlined below provide evidence consistent with contractional versus extensional deformation.

2.2. Bow-shaped ridge morphology

The shape of the ridges (the contact between a ridge and surrounding terrain) may record its movement history. Cassini SAR imagery clearly shows that many of Titan's ridges have a bow-shaped (arcuate) morphology (Figs. 1 and 3). These ridges found in Cassini flybys T8 and T61 (Figs. 1 and 3) have slightly asymmetric profiles in the form of closely paired bright and dark areas, indicative of radar illumination across a sharp topographic boundary, and have distinct fault-and-thrust morphologies (curvilinear traces and parallel groups of ridges). These may suggest that the ridge has a steeper slope on one side than the other, and that a possible low-angle thrust fault plane dips to the north (Fig. 3).

Contractional deformation typically produces arcuate structures. The leading edges of thrust faults are commonly curved in map view, typically convex toward the movement direction. If the ridges are formed by contractional processes, the 'bow-and-arrow rule' (Elliott, 1976) can be used to constrain the kinematic history of ridge belts on Titan. Elliott (1976) states that if the trace of a fault is pictured as a bow, an arrow strung on the string of that bow points in the direction the hanging wall moved (Fig. 3a) and displacement reaches a maximum in the central region (Fig. 3a). A Cassini SAR mosaic (Fig. 3b) shows a series of bright curvilinear ridges at 200°W, 10°S in Titan's equatorial region. By analyzing each scarp's concave direction, we can obtain the movement direction with the bow-and-arrow rule. Our analysis (Fig. 3b) shows the curved ridges in Cassini flybys T8 and T61 (Fig. 3b) have opposite directions of movement on the faults, which is expected due to the conjugate nature of many faults. The average fold width in this area is ~30 km and maximum displacement averages ~22 km for the ridges at 200°W, 10°S in Titan's equatorial region (Fig. 3).

Use of these surface morphology patterns to understand the geometry and kinematics of faulting adds significantly to evidence from previous studies (e.g., Mitri et al., 2010a,b; Radebaugh et al., 2011; Solomonidou et al., 2013; Liu et al., this issue) for the formation of equatorial ridges on Titan by contraction.

3. Strength of Titan's lithosphere

The role of contractional tectonism on Titan depends greatly on the strength of Titan's lithosphere. The strength of the upper lithosphere is primarily controlled by increasing lithostatic pressure with depth according to Byerlee's law (Byerlee, 1978). As temperature increases in the lower part of the lithosphere, strength decreases with depth and deformation is controlled by ductile flow. The composition of Titan's crust is mainly water ice, perhaps mixed with methane hydrate at shallow depths (Lunine and Lorenz, 2009). Here, we analyze the mechanical behavior of ice according to Byerlee's law to estimate the conditions for brittle failure of Titan's upper lithosphere (Byerlee, 1978; Beeman et al., 1988). The yield stress envelope for this case (Watts, 2001; Luttrell and Sandwell, 2006) is:

$$\sigma_c = k\rho g z \tag{1}$$

where σ_c is the stress for contraction, ρ is the density of ice, g is the acceleration of gravity, z is the depth, and the dimensionless factor $k = 2.6$ is a constant from the application of Byerlee's law to water ice (Watts, 2001; Luttrell and Sandwell, 2006). The crustal parameters of Titan are summarized in Table 2.

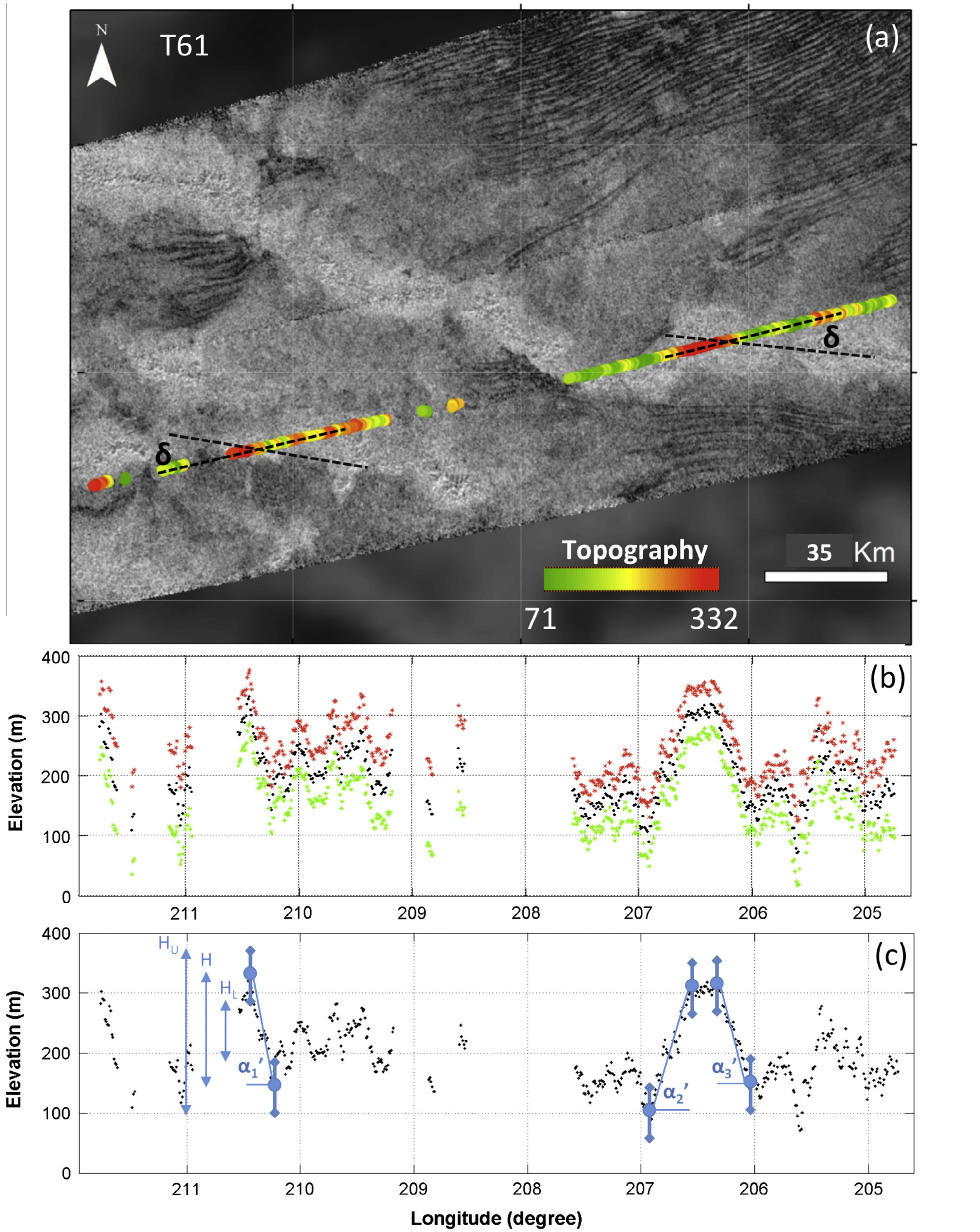

Fig. 2. Slope measurement of ridges on Titan. A SARTopo trace (colored line) is shown on the Cassini SAR T61 flyby swath with topographic relief profiles. Vertical exaggeration is 250: 1. (a) The coordinates of the center of this image are 208.3°W, 3.4°S. α' is the apparent slope or the average slope obtained from the SARTopo profile and δ is the angle between the line of mountain strike and the line of SARTopo trace. (b) Topographic profile with uncertainty extracted from SARTopo datasets. Black points represent the SARTopo height data. Red points represent the upper bound of height uncertainty in their along-track and vertical position. Green points are the height uncertainty lower bound. The size of each point is determined by its associated along-track and across-track errors. (c) Topographic relief profile marked (in blue color) with the locations of the ridge peak and floor elevations. H is measured ridge height; H_L is ridge height lower bound and H_U is ridge height upper bound. Description of slope measurement procedure is in Section 2.1. The true slopes α for folds from left to right are 1.8°, 1.9° and 1.5°, respectively. The details of the calculated slope angles and uncertainty for each measurement can be found in Table 1. (For interpretation of the references to color in this figure legend, the reader is referred to the web version of this article.)

Table 1
Slope measurements of possible fold belts on Titan.

#	Location	SAR flyby swath	H (m)	H_L (m)	H_U (m)	W (km)	α' (°)	δ (°)	α (°)	α uncertainty (°)
1	(207.4°W, 4.0°S)	T61	180	97	263	15 ± 10	0.7	23	1.8	0.6–7.7
2	(210.4°W, 4.6°S)	T61	250	166	334	22 ± 10	0.6	20	1.9	0.9–4.7
3	(210.4°W, 4.6°S)	T61	150	72	228	20 ± 10	0.4	20	1.5	0.4–3.8

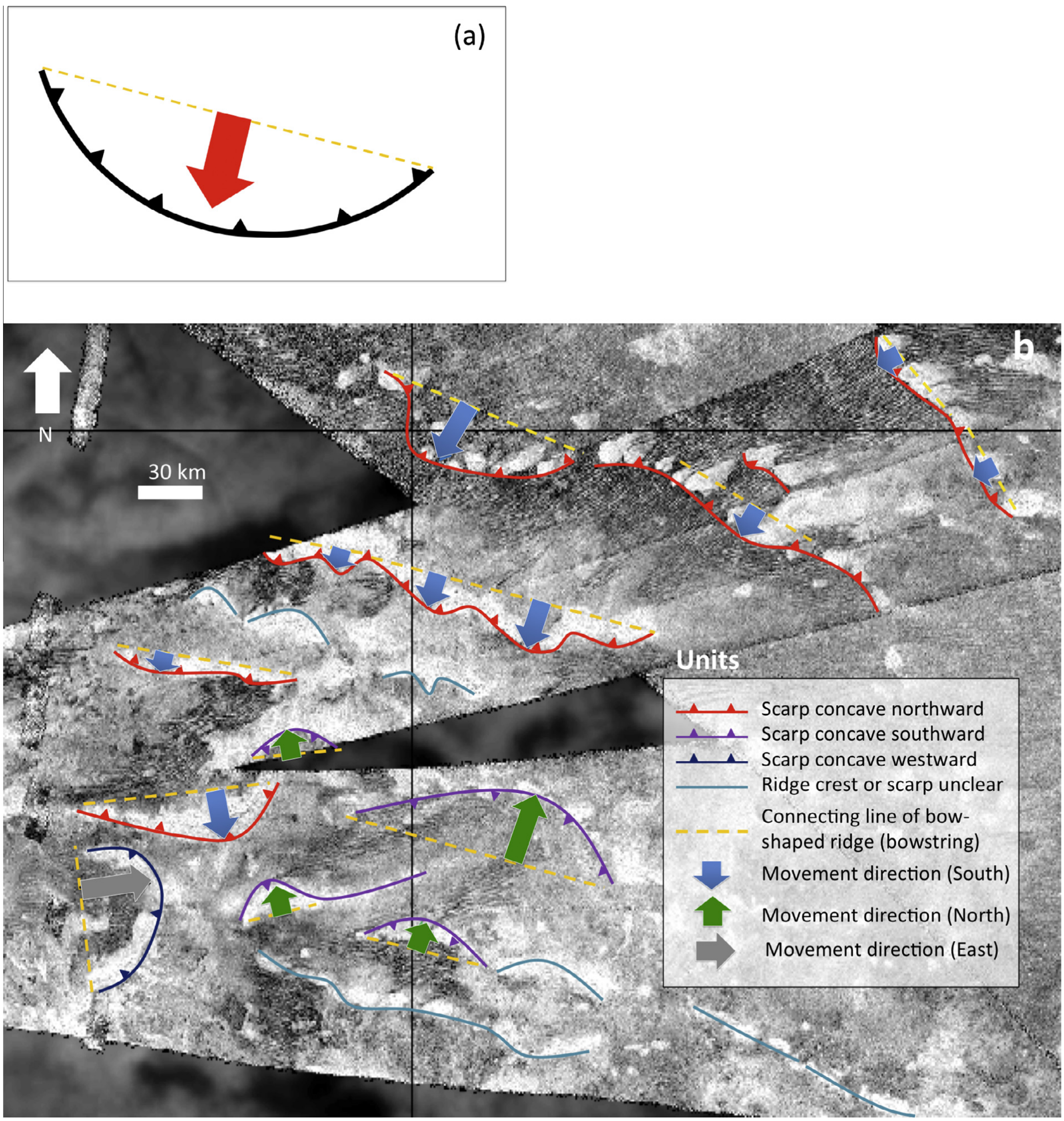

Fig. 3. Morphological analysis of equatorial ridge belts using the "bow and arrow" rule. (a) Schematic diagram illustrating the bow-and-arrow rule of Elliott (1976). In plan view, the trace of the thrust fault is arcuate and the edges of the thrust sheet are regions of shear deformation. Displacement reaches a maximum as red arrow extends in the central region. (b) A Cassini SAR mosaic (T8, T61 and T41 flyby swaths) with ridge scarp traces, which are shown as lines with teeth. Each line represents the trend of the basal scarp of a single ridge (i.e., fault strike), and the teeth point in the inferred dip direction of an underlying low-angle thrust fault plane. Ridge belts (200°W, 3°S) are arcuate colored by the scarp-concave direction: northward (red), southward (purple), and westward (blue), respectively. The yellow dashed lines are 'bowstrings', which represent the initial position of thrust fault. The fault propagated from near the tail of the arrow laterally along the yellow line to the ends of the 'bow' where the displacement is zero. The blue or green 'arrows' show the inferred direction and distance the hanging wall moved during thrusting from its initial position of the yellow line (i.e., maximum displacement). All of these features suggest contraction. (For interpretation of the references to color in this figure legend, the reader is referred to the web version of this article.)

Please cite this article in press as: Liu, Z.-Y.C., et al. Role of fluids in the tectonic evolution of Titan. Icarus (2016), http://dx.doi.org/10.1016/j.icarus.2016.02.016

Table 2
Crustal parameters of Titan.

Parameter	Description	Value	Reference
ρ	Density of lithosphere (Ice I)	900 kg m^{-3}	Tobie et al. (2005)
g	Acceleration due to gravity	1.35 m s^{-2}	Iess et al. (2010)
ρ_f	Density of the hydrocarbon fluid	600 kg m^{-3}	Lorenz (2002)
C	Cohesion	1.0 MPa	Beeman et al. (1988)

The ductile behavior of the lower part of Titan's lithosphere is assumed to follow the constitutive rheology of viscous flow as based on laboratory measurements (Durham et al., 1997; Goldsby and Kohlstedt, 2001). The yield stress envelope can be described in terms of the strain rate ε, based on the flow law of Durham and Stern (2001):

$$\sigma = \left|\frac{\varepsilon}{Ad^{-m}e^{\left(\frac{-Q}{RT}\right)}}\right|^{\frac{1}{n}} \tag{2}$$

where A is a material-dependent constant, d is the grain size, m is the grain-size exponent, n is a power-law exponent, Q is the activation energy for creep, R is the gas constant, and T is the absolute surface temperature. We assume a surface temperature of 94 K (Tobie et al., 2005), gas constant of 8.31 J mole^{-1} K^{-1} (Durham et al., 1997) and a reasonable range of temperature gradients of 5 K km^{-1} (Jaumann et al., 2010) and 10 K km^{-1} (Mitri et al., 2010a,b). The ice grain size is not well constrained, so we adopt a grain size of 0.1–1 mm to be consistent with the current literature for icy satellite tectonics (e.g., McKinnon, 2006; Bland and Showman, 2007). Goldsby and Kohlstedt (2001) summarized ice rheology for a range of stresses, temperatures and grain sizes. For ice I, dislocation creep (regime A, B and C) is typically associated with large stresses. However, Durham and Stern (2001) argued that dislocation creep regime C can be mostly ignored for icy moons. In addition, since the modeled ice shell temperature range is <240 K for Titan (Mitri et al., 2010a), the rheology of ductile B creep rather than regime A is more appropriate for the case of Titan and is consistent with the literature dealing with icy satellites (e.g., Durham and Stern, 2001; Pappalardo and Davis, 2007). By comparison, grain size-sensitive creep (grain boundary sliding, or GBS) and basal slip (BS) are generally associated with smaller stresses and slower strain rates. Grain boundary sliding (GBS) flow is limited by the basal slip (BS) mechanism such that the slower of the two mechanisms controls the flow. Thus, we adopt (1) dislocation creep (regime B), (2) grain boundary sliding (regime GBS), and (3) basal slip (regime BS) to estimate the ductile strength of Titan's lower lithosphere (Eq. (2)). Each deformation mechanism has corresponding experimental values for the parameters A, m, n, and Q. The rheological parameters of phase I ice used in this work are summarized in Table 3.

Brittle strength depends strongly on pressure, but weakly on temperature, and so increases with depth (Eq. (1)). Ductile strength depends mainly on temperature, and so decreases with depth (Eq. (2)). Here we follow Durham and Stern (2001) to generate Titan's lithospheric strength profile by plotting both brittle and ductile trends as strength verse depth, assuming reasonable ranges of geothermal gradients (5 K km^{-1} and 10 K km^{-1}) and fixing strain rates (10^{-14}, 10^{-15} and 10^{-16} s^{-1}). We apply a range of plausible strain rates in order to assess the sensitivity of the results to the assumed strain rate and to insure our results are comparable to previous studies (e.g., Durham and Stern, 2001; Pappalardo and Davis, 2007; Mitri et al., 2010a,b). Of particular relevance to our work, Mitri et al. (2010a,b) suggested a strain rate of $\sim10^{-15}$ s^{-1} can produce the mountains on Titan with the same scale as our observations. Thus our spread in strain rates is centered on this observation-based value.

Table 3
Rheological parameters used in Eq. (2).

Creep regime	Log$A$ (MPa^{-n} m^{m} s^{-1})	m	n	Q (kJ mole^{-1})
B	5.1	0	4.0	61
GBS	−2.4	1.4	1.8	49
BS	7.74	0	2.4	60

Durham and Stern (2001).

Fig. 4 illustrates Titan's lithospheric strength as a function of depth in the brittle and ductile regimes, with the maximum lithospheric strength approximated by the intersection of the brittle line and ductile failure curves. Titan's lithospheric strength in contraction is ~7–10 MPa for regime B with a temperature gradient of 5 K km^{-1} and ~4–6 MPa with a temperature gradient of 10 K km^{-1}, which corresponds to a higher heat flux (Fig. 4a). The estimation based on deformation regime B is comparable to estimates for Ganymede's lithospheric strength of ~10–11 MPa with low heat flux and ~6–7 MPa with high heat flux (Durham and Stern, 2001; Pappalardo and Davis, 2007). In addition, there is smaller lithospheric strength in contraction of ~6–9 MPa and ~4–7 MPa with a temperature gradient of 5 K km^{-1} for GBS and BS respectively, and ~3–5 MPa with a higher temperature gradient of 10 K km^{-1} for both GBS and BS (Fig. 4b and c). In summary, to enable contractional strain on Titan, a stress of up to 4–10 MPa is required, much greater than the known sources of stress on Titan (<0.1 MPa). Note that a grain size of 1.0 mm is used for the results shown in Fig. 4. A more complete sensitivity analysis of grain size, strain rate and thermal gradients is present in Section 4.4.

4. Pore fluid pressure enables contractional tectonism

4.1. Earth

On Earth, some thrust faults exist that require horizontal motions of thrust sheets over distances as great as 100 km. However, the stresses needed to move the thrust sheets up thrust ramps and along thrust flats exceed the crushing strengths of even the strongest rocks, therefore yielding a strength paradox, similar to the one evident on Titan. This paradox was resolved by Hubbert and Rubey (1959) who demonstrated that high fluid pressures can nearly cancel out the normal stress component on a fault plane thereby significantly reducing frictional resistance to sliding. Solving the paradox involved modifying the Mohr–Coulomb law of frictional shear strength:

$$\tau = \mu(\sigma_N - P_f) + C \tag{3}$$

where τ is the shear stress required to cause slip, C is cohesion, μ is the coefficient of internal friction, σ_N is normal stress, and P_f is fluid pore pressure. Where fluid is unable to escape from a porous but impermeable subsurface horizon, fluid pressure (P_f) can build to the point of supporting most of the weight of the overlying rock. In other words, the fluid pressure is high enough to offset nearly all the normal stress (σ_N). Consequently, the shear stress (τ) needed to form a thrust fault must only exceed the cohesive strength (C) of rock. Under these conditions a small contractional stress can easily overcome the frictional strength of a material to form thrust sheets and related folds.

It should be noted that Price (1988) extended an alternative for the formation of thrusts arguing that significant strength heterogeneity and anisotropy in the upper lithosphere results in cumulative microthrusting events, where the compressional stress never has to exceed the crushing strength on the scale of an entire thrust sheet. Since the purpose of this paper is to examine the role of fluids, we do not discuss this model further, but acknowledge that

Please cite this article in press as: Liu, Z.-Y.C., et al. Role of fluids in the tectonic evolution of Titan. Icarus (2016), http://dx.doi.org/10.1016/j.icarus.2016.02.016

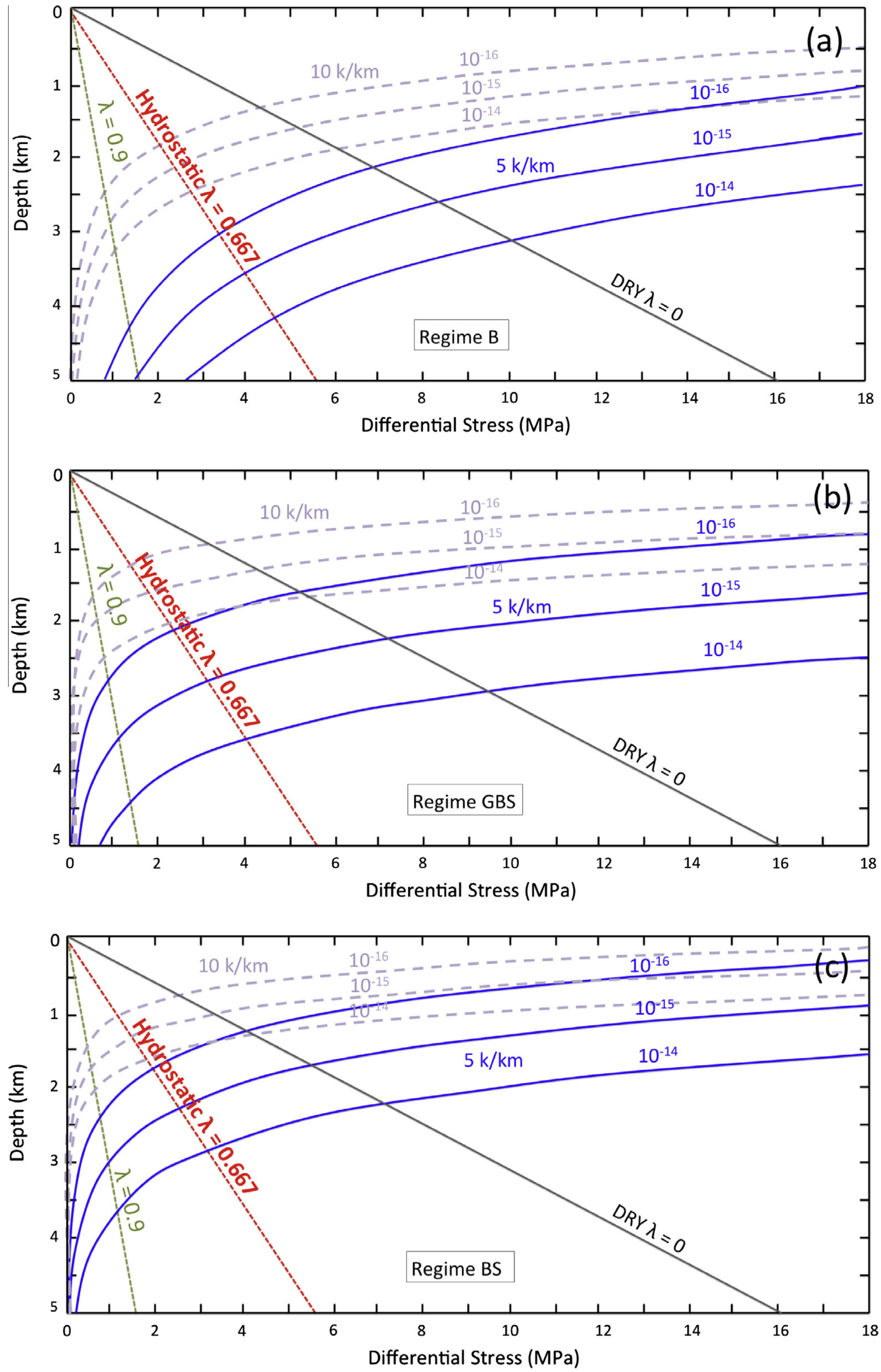

Fig. 4. Titan's lithospheric strength as a function of depth in the brittle and ductile regimes. Brittle failure lines (black, red, and green) show lithospheric strength for contraction under different conditions. The black line represents the strength with no fluid effects ($\lambda = 0$); the red dashed line is for moderate hydrostatic fluid pressure ratio ($\lambda = 0.67$); and the green dashed line is for a high fluid pressure ratio ($\lambda = 0.9$). Ductile strength curves (in blue and purple) for ice use ductile creep, a surface temperature of 94 K, and thermal gradient of 5 K km^{-1} and 10 K km^{-1} at various strain rates (10^{-14}, 10^{-15}, and 10^{-16} s^{-1}). Grain size of 1.0 mm is used here. The maximum lithospheric strength is approximated by the intersection of a brittle and a ductile failure curve. (a) Lithospheric strength profile in ice I phase dislocation creep B regime. The maximum lithospheric strength for a 'dry' lithosphere and a rapid strain rate of 10^{-14} s^{-1} is about 10 MPa with thermal gradient 5 K km^{-1}; for a high pore fluid pressure and low strain rate, the strength is <1 MPa. (b) Lithospheric strength profile in ice I phase basal slip-accommodated grain boundary sliding (GBS). (c) Lithospheric strength profile in ice I phase grain boundary sliding-accommodated basal slip (BS). For a high pore fluid pressure and low strain rate, the lithospheric strength is <1 MPa in both GBS and BS. Note that varying strain rates between 10^{-14} and 10^{-16} s^{-1} decreases the estimated lithospheric strength by ~30% to 40% in the three deformation regimes. (For interpretation of the references to color in this figure legend, the reader is referred to the web version of this article.)

future work may address its application to Titan's crustal environment.

4.2. Titan

Titan's upper icy crust is likely porous due to meteorite impacts, tectonism, and inclusions of methane clathrate hydrates (Lunine and Lorenz, 2009; Janssen et al., 2009; Neish et al., 2015a). It is also possibly filled with hydrocarbon fluid in a hydrocarbon-based hydrologic system (Lunine and Lorenz, 2009; Turtle et al., 2011). We adapt the Mohr–Coulomb Eq. (3) for Titan and assume pore fluid pressures (P_f) are locally high enough to offset all normal stresses (σ_N) as is the case along many faults on Earth. The cohesive strength (C) of Titan's fractured, icy crust may be about 1 MPa or smaller (Beeman et al., 1988). Based on Eq. (3), $\sigma_N - P_f = 0$, resulting in $\tau = C$. Thus, to enable brittle contractional strain on Titan, large stresses (4–10 MPa) are not necessary if the crust contains trapped pore fluids. Shear stresses (τ) of just 1 MPa or less are sufficient to overcome the cohesive strength of ice and form fold and thrust belts on Titan.

4.3. Pore fluid pressure ratio

Another important aspect of crustal fluids on Titan is the pore fluid pressure ratio (λ). Hydrostatic pressure in an aquifer corresponding to a pore fluid pressure ratio (λ) is defined as $\lambda = \rho_f/\rho_s$, also called the fluid pressure gradient (Davis et al., 1983), where ρ_f is the density of the fluid and ρ_s is the density of the crust. We can revise Eq. (3) in terms of the fluid pressure gradient (λ) (modified from Davis et al., 1983):

$$\tau = C + \mu\sigma_N^* = C + \mu\sigma_N(1-\lambda) \tag{4}$$

where σ_N^* is the effective normal stress fraction, the fractional value for normal stress remaining after it has been reduced by fluid pore pressure. On Earth, with a fluid (liquid water) density of 1 g/cm^3 and a crustal density of 2.5 g/cm^3, the hydrostatic pore fluid pressure ratio λ is ~0.4. Based on Eq. (4), hydrostatic pore pressure reduces the normal stress, leaving an effective normal stress fraction (σ_N^*) ~60% of the original value. On Titan, with a fluid (liquid methane) density of 0.6 g/cm^3 (Lorenz, 2002) and an icy crust density of 0.9 g/cm^3 (Tobie et al., 2005), the pore fluid pressure ratio λ is ~0.67, about 1.5 times greater than that for rocks on Earth. Thus, hydrostatic pore pressure on Titan reduces the normal stress to an even greater degree than on Earth, leaving an effective normal stress fraction (σ_N^*) ~33% of the original value. On Titan, where crustal conditions create a higher hydrostatic fluid pressure gradient (λ), there is a greater reduction in shear stress needed to enact brittle strain, which makes the formation of contractional structures even easier on Titan than on Earth.

Below most terrestrial fold-and-thrust belts, if permeability is restricted and fluid is trapped, pore pressures may exceed the hydrostatic pressure and the fluid becomes overpressured (Davis et al., 1983). The fluid pressure gradient may exceed the hydrostatic fluid pressure ratio ($\lambda > 0.4$ for Earth and $\lambda > 0.67$ for Titan). In Earth's crust, it is common to have a fluid pressure ratio $\lambda > 0.4$ (Davis et al., 1983). Thus, pore fluid pressure ratios below Titan's fold belts may also exceed the hydrostatic pressure and reach even higher values of λ. In addition, Mousis and Schmitt (2008) suggest the presence of clathrates of methane and water within the crust reduces its permeability by closing pore space networks connecting to the surface. This decrease in permeability would increase pore fluid pressures, reducing the shear strength of Titan's crust. Experimental studies are needed to determine how Titan's icy crust and hydrocarbon liquids chemically interact and what effect these mixtures have on crustal strength.

The failure strength of Titan's lithosphere with various fluid pore pressures can be calculated by Eqs. (3) and (4); the hydrostatic fluid pore pressure ($\lambda \sim 0.67$) reduces the maximum differential stress needed to enact contractional failure to ~3–5 MPa in regime B and ~2–4 MPa in GBS and BS (Fig. 4). With higher pore fluid pressure ($\lambda \sim 0.9$), the stress needed to form contraction decreases significantly, to ~1 MPa in regime B and <1 MPa for both GBS and BS (Fig. 4). Note that the relative strength of principal stresses determines the style of faulting, and that thrust faulting and principal stress modification due to pore overpressure is in agreement with a horizontal maximum compressive stress (Anderson, 1951).

4.4. Sensitivity analysis

The above results of lithospheric strength and fluid effects are based on a particular set of parameters (Tables 2 and 3) in Eqs. (1) and (2), some of which are poorly constrained, so it is important to investigate the sensitivity of the results to variations in these parameters. First, the factors influencing the brittle behavior of ice are relatively well constrained by experimental studies and do not significantly affect the results. However, the factors influencing the ductile strength curves are less well-constrained and could affect the estimated lithospheric strength in contraction. The parameters in the flow law (Eq. (2)), such as A (material-dependent constant), m (grain-size exponent), n (power-law exponent), Q (activation energy for creep), and R (gas constant), were determined by laboratory experiments (e.g., Durham et al., 1997; Goldsby and Kohlstedt, 2001), which have been widely used in models of icy satellite tectonics; thus, these parameters are not included in our sensitivity analysis. Grain size (d), however, is poorly constrained; we adapt a range of $d \sim 0.1$–1 mm to simulate the ductile strength curve in the deformation profile (Fig. 5) for three ice I regimes (B, GBS, and BS). We also use two different temperature gradients for the calculations: 5 K km^{-1} and 10 K km^{-1}. Fig. 5 illustrates how these two factors (grain size and temperature gradient) change the ductile strength curves. Regime B and BS (basal slip) are independent of grain size (as Fig. 5a and c shows). This is expected given the grain size exponent of regimes B and BS is zero. GBS (grain boundary sliding) depends inversely on grain size (as Fig. 5b shows). Decreasing the grain size from 1 mm to 0.1 mm would decrease the estimated lithospheric strength by ~30% in the GBS regime (and is similar for all three strain rates). However, grain size tends to increase in older glacial ice and in ice that has undergone substantial creep. Thus, the larger grain sizes, and increased lithospheric strength, are a more likely scenario. Increasing the temperature gradient from 5 K km^{-1} to 10 K km^{-1} would also decrease the estimated lithospheric strength by ~30% in the three deformation regimes. In addition, based on Fig. 4, varying strain rates between 10^{-14} and 10^{-16} s^{-1} decreases the estimated lithospheric strength similarly by ~30–40% in the three deformation regimes. Importantly, uncertainties in the input parameters have a negligible effect on our main conclusion since the full spread in applied grain sizes, temperature gradients, strain rates, and constants are consistent with the fact that the differential stress needed to enact contractional failure is significant. Moreover, if contractional tectonism occurred early in the history of Titan when the heat flux from the interior was higher, this would decrease the lithospheric strength and also facilitate the formation of folds and contractional tectonism. However, based on the calculations above, fluid pore pressure is more effective at facilitating the formation of contractional features than higher heat flux. Therefore, our conclusion that pore fluid pressure facilitates the formation of contractional features on Titan is robust. Along with this conclusion, and in combination with the observations of the

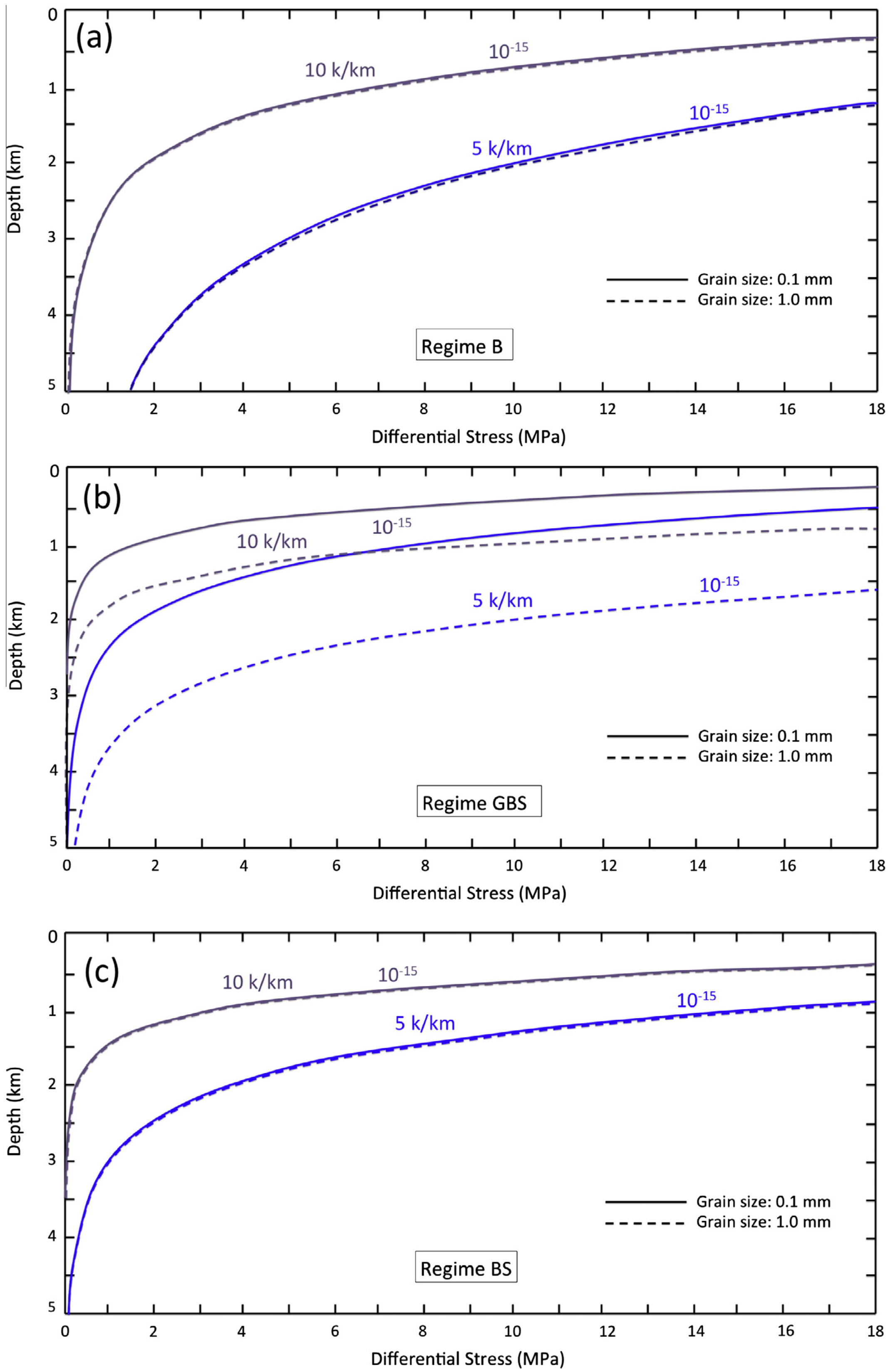

Fig. 5. Sensitivity analysis on model parameters: grain size and temperature gradient. (a) Ductile strength profile in dislocation creep regime B with temperature gradients: 5 K km^{-1} (blue curves) and 10 K km^{-1} (purple curves), and grain size: 0.1 mm (solid line) and 1.0 mm (dash-line) at strain rate of 10^{-15} s^{-1}. (b) Ductile strength profile in GBS. (c) Ductile strength profile in BS. Sensitivity analysis shows that regime B and BS are independent of grain size; GBS depends inversely on grain size. Altering grain size from 1 mm to 0.1 mm would decrease the estimated lithospheric strength by ~30% in GBS regime. The sensitivity of the results to grain size is very similar for all strain rates, thus only 10^{-15} s^{-1} is shown here. Increasing temperature gradient from 5 K km^{-1} to 10 K km^{-1} would also decrease the estimated lithospheric strength by ~30% in three deformation regimes (also shown in Fig. 4). (For interpretation of the references to color in this figure legend, the reader is referred to the web version of this article.)

Please cite this article in press as: Liu, Z.-Y.C., et al. Role of fluids in the tectonic evolution of Titan. Icarus (2016), http://dx.doi.org/10.1016/j.icarus.2016.02.016

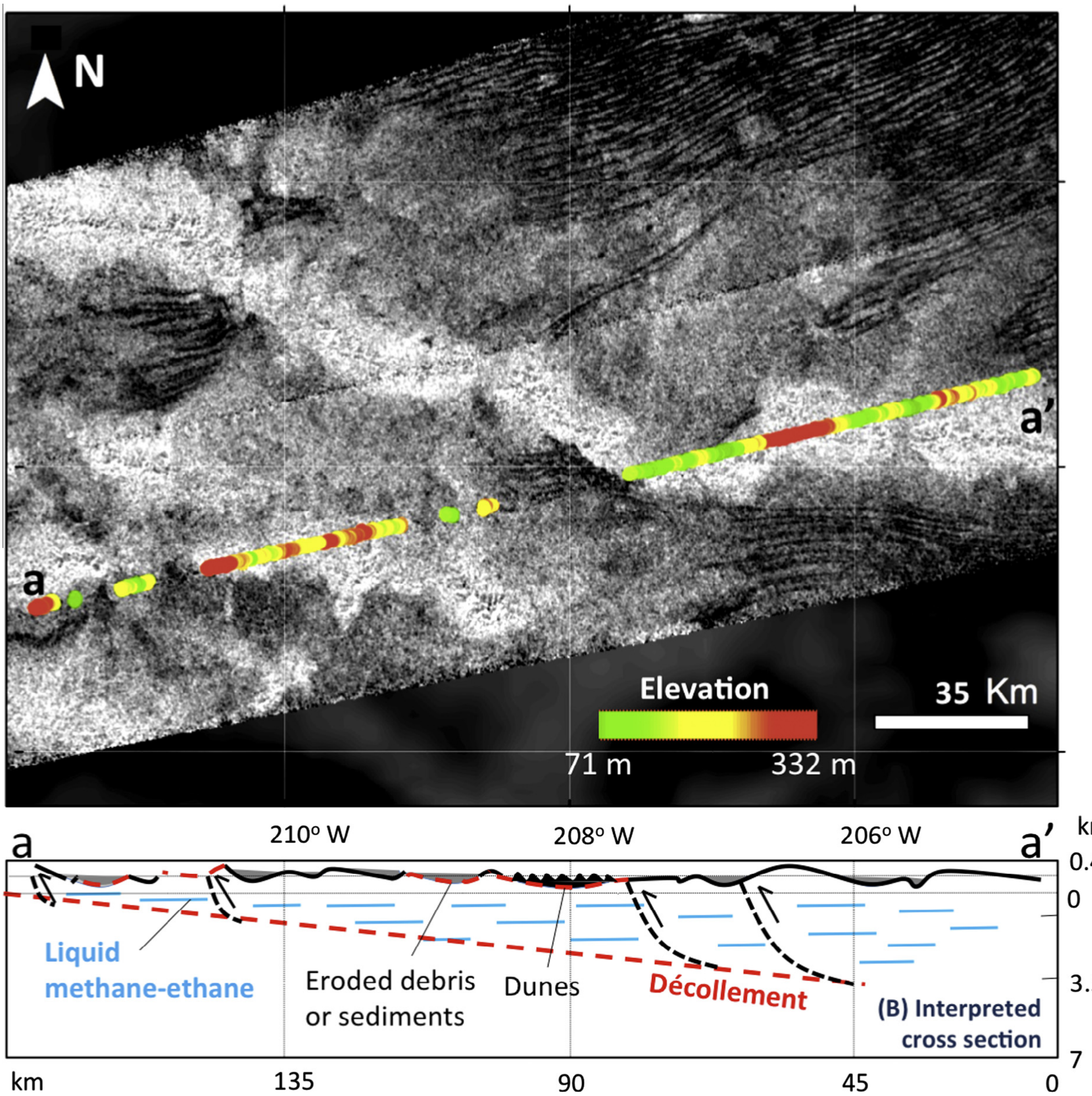

Fig. 6. The topography and interpreted cross-section of an equatorial ridge belt on Titan. A SARTopo profile (colored line, coded by elevation) is shown on the Cassini T61 flyby swath. Radar-bright curvilinear features are ridge belts. Radar black lines are sand dunes, which are stopped by the higher elevation ridges. In profile a–a′, the black line is the actual elevation extracted from SARTopo data and the red dashed line is the interpreted topography. Vertical exaggeration of topographic profile portion (0–0.4 km) is: 50:1. The short blue lines represent crustal hydrocarbon (methane and ethane) fluids trapped in pore spaces. The gray patches at the surface represent eroded debris and sediment accumulated between the ridges. The interpretive cross section a–a′ assumes that thin-skinned tectonics are appropriate for Titan and shows a series of imbricate thrust faults splaying upward from a basal décollement beneath surface folds. Vertical exaggeration of subsurface cross section (0–7 km) is: 5:1. (For interpretation of the references to color in this figure legend, the reader is referred to the web version of this article.)

morphology of ridges (Section 2), we explore the possible type of contractional tectonism on Titan in the next section.

5. Titan's style of deformation: thin-skinned tectonics

Since hydrocarbon liquids are likely present in the shallow part of Titan's crust (2–3 km) (Lunine and Lorenz, 2009; Choukroun et al., 2010), faults and associated crustal deformation do not need to involve the entire thickness of the icy crust. Thus, the proper conditions may exist for thin-skinned tectonics as implied by the presence of ridge belts. In this style of tectonic deformation, when a crustal section with fluid overpressures is subjected to a large enough horizontal maximum compressive stress, it deforms internally and forms low-angle thrust faults that branch upward from a basal slip surface (décollement). Movement along the faults causes hanging wall thrust sheets to develop fold geometries that relate directly to fault geometry.

The lower boundary of the décollement depth is $\sim w \tan\theta$, where w is the fold width, θ is the wedge angle = $\alpha + \beta$, α is the surface slope and β is the décollement dip angle (Davis et al., 1983). We estimated fold width from Cassini SAR images by measuring the width of ridge belts (Section 2.2), which are visible as SAR-bright linear features because they are rough and fractured, in contrast to surrounding SAR-dark and smooth or fine-grained sandy terrains (Radebaugh et al., 2007; Liu et al., 2012). For the fold-and-thrust belts located at 200°W, 10°S on Titan (Fig. 1), the surface slope α is ~1.5–2° (Table 1). The width of a single fold is ~30 km. The décollement dip angle (β) cannot be obtained with

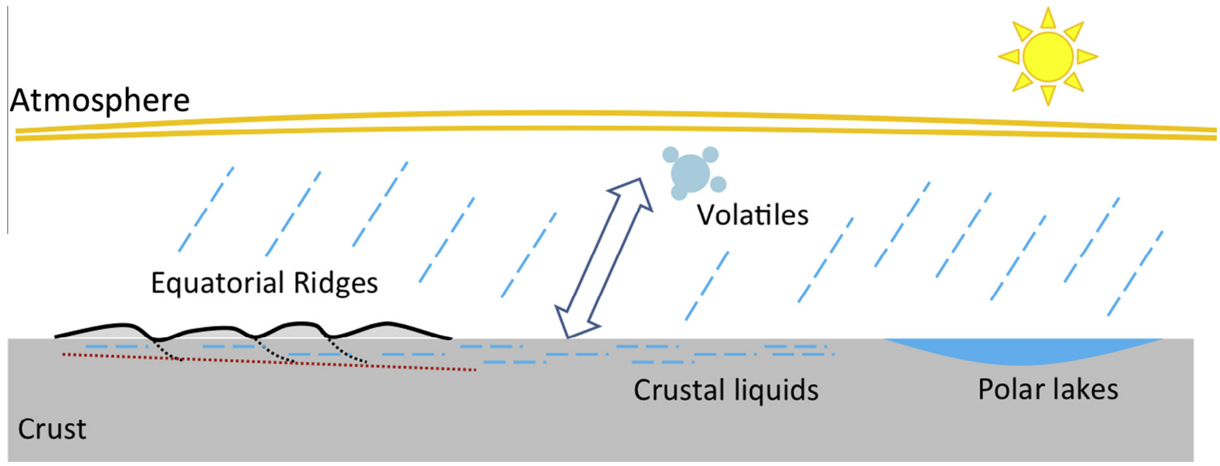

Fig. 7. The effect of fluids and atmosphere on the possible development of contractional deformation on Titan. Schematic diagram illustrating that Titan's relatively thick atmosphere has provided and stabilized crustal liquids. The short blue lines represent hydrocarbon fluids trapped in pore spaces. The resultant fluid overpressures in the shallow crust may weaken it and facilitate the formation of contractional features, basal décollements (red dashed line), and thrusts and folds. The presence of crustal fluids thus affects the structural evolution. (For interpretation of the references to color in this figure legend, the reader is referred to the web version of this article.)

the current Cassini topography data. On Earth, $0° < \beta < 10°$ is considered to be a reasonable range for thrust faults (Davis et al., 1983). Here we adopt this range of dip angles to estimate the décollement depth. Using the estimated values of w, α and β, the lower boundary of the décollement depth would be approximately 2–3 km. The calculated décollement depths of 2–3 km lie above the calculated depth of the brittle–ductile transition (Fig. 4), and are consistent with thin-skinned deformation on Titan.

Using the topographic profile of the fold belt, the estimate of décollement depth, and the assumption of high pore fluid pressure with thin-skinned tectonics, we are able to construct a generalized cross-section of Titan's ridge belts at 200°W, 10°S (Fig. 6). In the thin-skinned model, the upper crust is detached from the underlying basement along fault planes with a ramp-flat geometry; thus, the thrusting angle should be higher than the overall slope angle of the fold belts. Note that the analyzed ridges here are the only parallel ridges with SAR topographic data available. There are other parallel ridges on Titan but they either have no topographic data or are out of current SAR coverage.

6. Discussion

Titan may be the only icy satellite on which there is strong morphological evidence for contractional deformation. What makes Titan unique? Mitri et al. (2010a) suggest that icy satellites without high-pressure phases of water ice layers (e.g., Europa) experience global extension due to expansion of the icy crust during progressive cooling. In contrast, Titan is larger and it should have developed high-pressure ices, which could lead to global contraction during internal cooling. In this study, we show that fluid overpressures provide a way to significantly reduce the strength of Titan's crust so as to allow contractional deformation at much lower stresses. We therefore presume that the pair of conditions—high-pressure ice phases inducing contraction and a low-density crustal fluid—is necessary for contractional mountain building.

Titan's formation at greater distances from the Sun and at lower temperatures allowed for the incorporation of significant amounts of ammonia and methane ices compared to the icy jovian satellites. Because of this extra volatile endowment, Titan has a thick, nitrogen-rich atmosphere, which, because of its density (and the ambient temperature) stabilized liquid hydrocarbons and established a hydrocarbon-based hydrologic system complete with liquids flowing on and below its surface (Fig. 7). Thus, through geological time, Titan's thick atmosphere has sustained the stability of surface and subsurface liquids, leading to the weakening of the upper crust. Thus, the volatile component obtained during accretion may directly affect the style of tectonics and its evolution on Titan, just as it does on Earth.

The facilitation of possible thrust faults on Titan through the presence of hydrocarbon liquids and resultant crustal weakening yields contractional features—fold and thrust belts—with morphologies similar to those on Earth (Radebaugh et al., 2007; Mitri et al., 2010a; Cook-Hallett et al., 2015; Liu et al., this issue). This similarity strengthens the case for ongoing comparisons of surface and near-surface processes on Titan and Earth. Moreover, we emphasize the necessity of accounting for fluid overpressures, resultant crustal weakening, and thin-skinned deformation when constructing models to explain the tectonic patterns of Titan. This study furthermore advances the understanding of how liquids, other than water, play an essential role in the tectonic evolution of icy satellites.

Finally, our conclusions highlight the significance of fluids in planetary lithospheres and the importance of atmospheres and initial compositions for the development of planetary tectonic systems. This in turn has implications for tectonic processes on all solid planetary bodies that may have fluids in their lithospheres, now or in the past.

Acknowledgments

We are grateful to all who developed and operate the Cassini–Huygens mission. Z.Y.-C.L. was supported by a Graduate Research Fellowship at Brigham Young University, USA. We thank Catherine Neish, who shared her SARTopo data processing code with us. Hendrik Lenferink provided helpful discussion of the strength of methane clathrate hydrate and ice mixtures. Two anonymous reviewers provided valuable suggestions for improving the manuscript.

References

Anderson, E.M., 1951. The Dynamics of Faulting. Oliver and Boyd, Edinburgh.
Banks, M.E. et al., 2012. Morphometric analysis of small-scale lobate scarps on the Moon using data from the Lunar Reconnaissance Orbiter. J. Geophys. Res.: Planets 117 (E12).
Beeman, M., Durham, W.B., Kirby, S.H., 1988. Friction of ice. J. Geophys. Res.: Solid Earth 93 (B7), 7625–7633. http://dx.doi.org/10.1029/JB093iB07p07625.

Beuthe, M., 2010. East–west faults due to planetary contraction. Icarus 209 (2), 795–817. http://dx.doi.org/10.1016/j.icarus.2010.04.019.
Black, B.A. et al., 2012. Estimating erosional exhumation on Titan from drainage network morphology. J. Geophys. Res.: Planets 117 (E8). http://dx.doi.org/10.1029/2012JE004085.
Bland, M.T., Showman, A.P., 2007. The formation of Ganymede's grooved terrain: Numerical modeling of extensional necking instabilities. Icarus 189, 439–456. http://dx.doi.org/10.1016/j.icarus.2007.01.012.
Burr, D.M. et al., 2013. Fluvial features on Titan: Insights from morphology and modeling. Geol. Soc. Am. Bull. 125 (3–4), 299–321. http://dx.doi.org/10.1130/B30612.1.
Byerlee, J., 1978. Friction of rocks. Pure Appl. Geophys. 116 (4–5), 615–626.
Choukroun, M. et al., 2010. Stability of methane clathrate hydrates under pressure: Influence on outgassing processes of methane on Titan. Icarus 205 (2), 581–593. http://dx.doi.org/10.1016/j.icarus.2009.08.011.
Collins, G.C. et al., 2009. Tectonics of the outer planet satellites. Planet. Tectonics 11, 264–350.
Cook-Hallett, C. et al., 2015. Global contraction/expansion and polar lithospheric thinning on Titan from patterns of tectonism. J. Geophys. Res.: Planets 120 (6), 1220–1236. http://dx.doi.org/10.1002/2014JE004645.
Davis, D., Suppe, J., Dahlen, F.A., 1983. Mechanics of fold-and-thrust belts and accretionary wedges. J. Geophys. Res.: Solid Earth 88 (B2), 1153–1172.
Dombard, A.J., McKinnon, W.B., 2006. Folding of Europa's icy lithosphere: An analysis of viscous-plastic buckling and subsequent topographic relaxation. J. Struct. Geol. 28 (12), 2259–2269. http://dx.doi.org/10.1016/j.jsg.2005.12.003.
Durham, W.B., Stern, L.A., 2001. Rheological properties of water ice-applications to satellites of the outer planets. Annu. Rev. Earth Planet. Sci. 29 (1), 295–330. http://dx.doi.org/10.1146/annurev.earth.29.1.295.
Durham, W.B., Kirby, S.H., Stern, L.A., 1997. Creep of water ices at planetary conditions: A compilation. J. Geophys. Res.: Planets 102 (E7), 16293–16302. http://dx.doi.org/10.1029/97JE00916.
Elachi, C. et al., 2005. Cassini RADAR views the surface of Titan. Science 308 (5724), 970–974. http://dx.doi.org/10.1126/science.1109919.
Elliott, D., 1976. The energy balance and deformation mechanisms of thrust sheets. Philos. Trans. R. Soc. Lond. Ser. A, Math. Phys. Sci. 283 (1312), 289–312.
Goldsby, D.L., Kohlstedt, D.L., 2001. Superplastic deformation of ice: Experimental observations. J. Geophys. Res.: Solid Earth 106 (B6), 11017–11030. http://dx.doi.org/10.1029/2000JB900336.
Hayes, A. et al., 2008. Hydrocarbon lakes on Titan: Distribution and interaction with a porous regolith. Geophys. Res. Lett. 35 (9). http://dx.doi.org/10.1029/2008GL033409.
Hubbert, M.K., Rubey, W.W., 1959. Role of fluid pressure in mechanics of overthrust faulting I. Mechanics of fluid-filled porous solids and its application to overthrust faulting. Geol. Soc. Am. Bull. 70 (2), 115–166.
Iess, L. et al., 2010. Gravity field, shape, and moment of inertia of Titan. Science 327 (5971), 1367–1369. http://dx.doi.org/10.1126/science.1182583.
Janssen, M.A. et al., 2009. Titan's surface at 2.2-cm wavelength imaged by the Cassini RADAR radiometer: Calibration and first results. Icarus 200 (1), 222–239. http://dx.doi.org/10.1016/j.icarus.2008.10.017.
Jaumann, R. et al., 2010. Geology and surface processes on Titan. In: Titan from Cassini–Huygens. Springer, Netherlands, pp. 75–140. http://dx.doi.org/10.1007/978-1-4020-9215-2_5.
Liu, Z.Y.C. et al., 2012. Evidence for an endogenic origin of mountains on Titan Lunar Planet. Sci. 43. Abstract 2378 (Houston, TX).
Liu, Z.Y.C. et al., 2015. The tectonics of Titan: Global structural mapping from Cassini RADAR. Icarus. doi: http://dx.doi.org/10.1016/j.icarus.2015.11.021 (this issue).
Lorenz, R.D., 2002. Thermodynamics of geysers: Application to Titan. Icarus 156 (1), 176–183.
Lorenz, R.D. et al., 2008. Fluvial channels on Titan: Initial Cassini RADAR observations. Planet. Space Sci. 56 (8), 1132–1144. http://dx.doi.org/10.1016/j.pss.2008.02.009.
Lunine, J.I., Lorenz, R.D., 2009. Rivers, lakes, dunes, and rain: Crustal processes in Titan's methane cycle. Annu. Rev. Earth Planet. Sci. 37, 299–320.
Lunine, J.I. et al., 2008. Titan's diverse landscapes as evidenced by Cassini RADAR's third and fourth looks at Titan. Icarus 195 (1), 415–433. http://dx.doi.org/10.1016/j.icarus.2007.12.022.
Luttrell, K., Sandwell, D., 2006. Strength of the lithosphere of the Galilean satellites. Icarus 183 (1), 159–167. http://dx.doi.org/10.1016/j.icarus.2006.01.015.
McKinnon, W.B., 2006. On convection in ice I shells of outer Solar System bodies, with detailed application to Callisto. Icarus 183, 435–450. http://dx.doi.org/10.1016/j.icarus.2006.03.004.
Mitri, G., Pappalardo, R.T., Stevenson, D.J., 2010a. Evolution and interior structure of Titan. Lunar Planet. Sci. 41. Abstract 2229 (Houston, TX).
Mitri, G. et al., 2010b. Mountains on Titan: Modeling and observations. J. Geophys. Res.: Planets 115 (E10). http://dx.doi.org/10.1029/2010JE003592.
Mousis, O., Schmitt, B., 2008. Sequestration of ethane in the cryovolcanic subsurface of Titan. Astrophys. J. 677 (1), L67. http://dx.doi.org/10.1086/587141.
Neish, C.D. et al., 2015a. Spectral properties of Titan's impact craters imply chemical weathering of its surface. Geophys. Res. Lett. 42 (10), 3746–3754. http://dx.doi.org/10.1002/2015GL063824.
Neish, C.D. et al., 2015b. Fluvial erosion as a mechanism for crater modification on Titan. Icarus, doi: http://dx.doi.org/10.1016/j.icarus.2015.07.022 (this issue).
Paganelli, F. et al., 2010. Preliminary analysis of structural elements of Titan and implication for stress. Lunar Planet. Sci. 41. Abstract 2664 (Houston, TX).
Pappalardo, R.T., Davis, D.M., 2007. In: Workshop on Ices, Oceans, and Fire: Satellites of the Outer Solar System (LPI 1357, 2007), pp. 108–109.
Price, R.A., 1988. The mechanical paradox of large overthrusts. Geol. Soc. Am. Bull. 100 (12), 1898–1908.
Radebaugh, J. et al., 2007. Mountains on Titan observed by Cassini RADAR. Icarus 192 (1), 77–91.
Radebaugh, J. et al., 2011. Regional geomorphology and history of Titan's Xanadu province. Icarus 211 (1), 672–685. http://dx.doi.org/10.1016/j.icarus.2010.07.022.
Reidel, S.P., 1984. The Saddle Mountains; the evolution of an anticline in the Yakima fold belt. Am. J. Sci. 284 (8), 942–978.
Solomonidou, A. et al., 2013. Morphotectonic features on Titan and their possible origin. Planet. Space Sci. 77, 104–117. http://dx.doi.org/10.1016/j.pss.2012.05.003.
Stiles, B.W. et al., 2009. Determining Titan surface topography from Cassini SAR data. Icarus 202 (2), 584–598. http://dx.doi.org/10.1016/j.icarus.2009.03.032.
Stofan, E.R. et al., 2007. The lakes of Titan. Nature 445 (7123), 61–64. http://dx.doi.org/10.1038/nature05438.
Tewelde, Y. et al., 2013. Estimates of fluvial erosion on Titan from sinuosity of lake shorelines. J. Geophys. Res.: Planets 118 (10), 2198–2212. http://dx.doi.org/10.1002/jgre.20153.
Tobie, G. et al., 2005. Titan's internal structure inferred from a coupled thermal-orbital model. Icarus 175 (2), 496–502. http://dx.doi.org/10.1016/j.icarus.2004.12.007.
Turtle, E.P. et al., 2011. Rapid and extensive surface changes near Titan's equator: Evidence of April showers. Science 331, 1414–1417. http://dx.doi.org/10.1126/science.1201063.
Watts, A.B., 2001. Isostasy and Flexure of the Lithosphere. Cambridge University Press.

Please cite this article in press as: Liu, Z.-Y.C., et al. Role of fluids in the tectonic evolution of Titan. Icarus (2016), http://dx.doi.org/10.1016/j.icarus.2016.02.016